

Larissa Hütter*, Patrick H. Geoghegan, Paul D. Docherty, Milad S. Lazarjan, Donald Clucas and Mark Jermy

Fabrication of a compliant phantom of the human aortic arch for use in Particle Image Velocimetry (PIV) experimentation

DOI 10.1515/cdbme-2016-0109

Abstract: Compliant phantoms of the human aortic arch can mimic patient specific cardiovascular dysfunctions *in vitro*. Hence, phantoms may enable elucidation of haemodynamic disturbances caused by aortic dysfunction. This paper describes the fabrication of a thin-walled silicone phantom of the human ascending aorta and brachiocephalic artery. The model geometry was determined via a meta-analysis and modelled in SolidWorks before 3D printing. The solid model surface was smoothed and scanned with a 3D scanner. An offset outer mould was milled from Ebalta S-Model board. The final phantom indicated that ABS was a suitable material for the internal model, the Ebalta S-Model board yielded a rough external surface. Co-location of the moulds during silicone pour was insufficient to enable consistent wall thickness. The resulting phantom was free of air bubbles but did not have the desired wall thickness consistency.

Keywords: 3d scanning; additive manufacturing; experimental fluids; hemodynamics; particle image velocimetry.

1 Introduction

Cardiovascular disease (CVD) includes dysfunctions of the heart and blood vessels, including heart attacks, peripheral diseases at the artery and increased blood pressure.

***Corresponding author: Larissa Hütter**, Department of Mechanical Engineering, Karlsruhe Institute of Technology, Karlsruhe, Germany, E-mail: huetterlarissa@gmail.com

Patrick H. Geoghegan, Paul D. Docherty, Milad S. Lazarjan, Donald Clucas and Mark Jermy: Department of Mechanical Engineering, University of Canterbury, Christchurch, New Zealand, E-mail: patrick.geoghegan@canterbury.ac.nz (P.H. Geoghegan); paul.docherty@canterbury.ac.nz (P.D. Docherty); milad.soltanipourazarjan@pg.canterbury.ac.nz (M.S. Lazarjan); don.clucas@canterbury.ac.nz (D. Clucas); mark.jermy@canterbury.ac.nz (M. Jermy)

 © 2016 Larissa Hütter et al., licensee De Gruyter.

This work is licensed under the Creative Commons Attribution-NonCommercial-NoDerivs 4.0 License.

CVD killed 17.5 million people in 2012 and the World Health Organisation estimates 23.3 million people will die from CVD in 2030 [1, 2]. Circulatory dysfunction is a leading cause of ICU cost, admission and mortality [3–7].

Morphosis of the aortic structure during CVD ultimately leads to abnormal hemodynamics. However, the development and effect of the abnormal fluid dynamics during illness are not well known. *In vitro* experimentation has been touted as a potential method to elucidate hemodynamic dysfunction caused by disease of the aortic arch.

The challenge is to build patient specific models, which can predict and optimise the outcome of clinical treatments [8]. For these complex anatomical shapes, additive manufacturing allows construction of patient specific 3D models profiles using MRI and CT scans. Previous prototyping of the aorta for *in vitro* testing yielded rigid phantoms [9] (TangoPlus Stratasys). In contrast, Geoghegan et al. used an additive manufactured plaster internal mould and (CNC) milled aluminium external mould to produce a thin walled, compliant silicone phantom of the efferent artery that was a good match for *in vivo* conditions [10, 11]. The challenge of producing a thin walled model of the complex aortic geometry is presented in this research.

2 Methods and results

2.1 Phantom properties

A meta study of measurements of *in vivo* aortic geometry of healthy individuals was used to determine the dimensions of the phantom [12]. The aortic geometry was obtained from a meta-study of healthy individuals. The distensibility of the phantom was matched to reported values of aortic distensibility [10]. The model was scaled up by 50% to allow manufacture of thicker phantom walls (0.48 mm in the brachiocephalic artery and 0.99 mm in the aortic

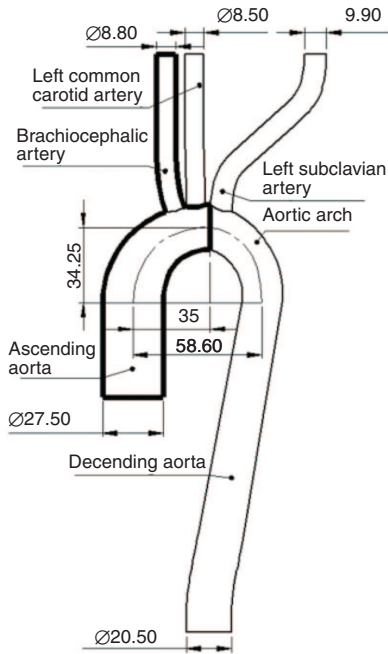


Figure 1: Internal geometry of the *in vivo* aorta. The black region depicts test phantom geometry.

arch). A preliminary model of the ascending aorta and the brachiocephalic artery was produced (Figure 1).

2.2 The internal mould

The model was divided into three parts and printed in low density on a Stratasys Dimension Elite using blue ABS plastic with a wall-thickness of 3 mm. The printing yielded a rough surface on the internal mould that was smoothed using 800-grit sandpaper and brief emersions in acetone (3 s followed by 20 s drying). The smoothed internal mould was scanned using an Artec Spider 3D scanner (published resolution of 100 μm) and processed using Artec Studio software. The software allows a comparison between the original CAD model and the manufactured internal mould (Figure 2). The internal mould had good horizontal fidelity but lower vertical fidelity due to the layering process involved in printing. The maximal deviation between the smoothed mould and the computational model was approximately 0.4 mm.

2.3 The external mould

Since the internal mould geometric deviation approached the proposed wall thickness in places, the external mould was modelled using offset 3D scan data from the internal

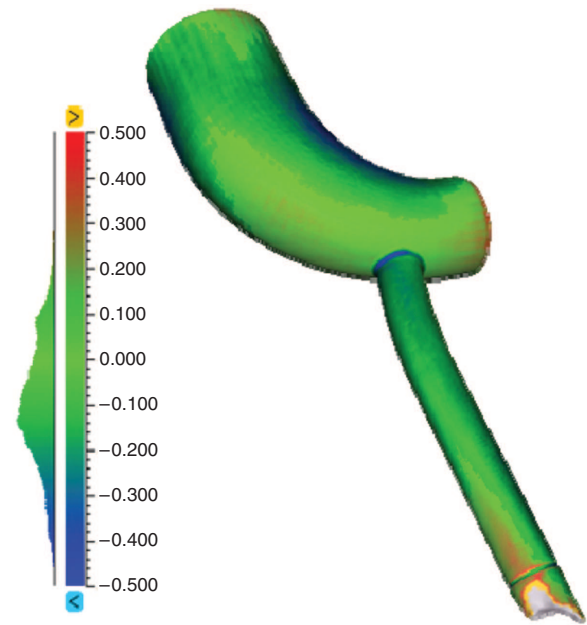


Figure 2: Deviation between CAD model and smoothed printed part (mm).

mould. Geomagic Design X was used to produce STL files with the correct geometry offsets. During import of the 3D scan mesh file, the “Mesh Build Up Wizard” was run and the “Region in Groups” tool was used. On these groups reference planes were inserted to build up enough planes to cover the whole model. On each plane a “Mesh Sketch” with 200 points of intersection of plane and scan file was made and splines interpolated between the intersections curves (Figure 3). A loft feature was applied to these splines to generate the transition geometry from the aortic arch to the brachiocephalic artery. The result is a solid CAD model of the same shape as the mesh that captured the imperfections caused by manufacturing of the internal mould (Figure 6).

A CNC 3-axis machining center milled the external mould geometry from Ebalta S-Model-board. The contact surfaces of the external mould were coated with an enamel spray paint to improve mould smoothness and limit silicone perfusion during curing.

Figure 4 shows the discrepancy between the finished external mould the computational model. While the greatest discrepancies are observed in the mounting plates and injection hole, the region of interest also contains discrepancies. In particular, there are significant changes in the wall of the aortic arch in one of the mould sections (0.3 mm). This error corresponds to a reduction of 30% of the intended wall thickness for the phantom. All regions of the brachiocephalic artery were well formed.

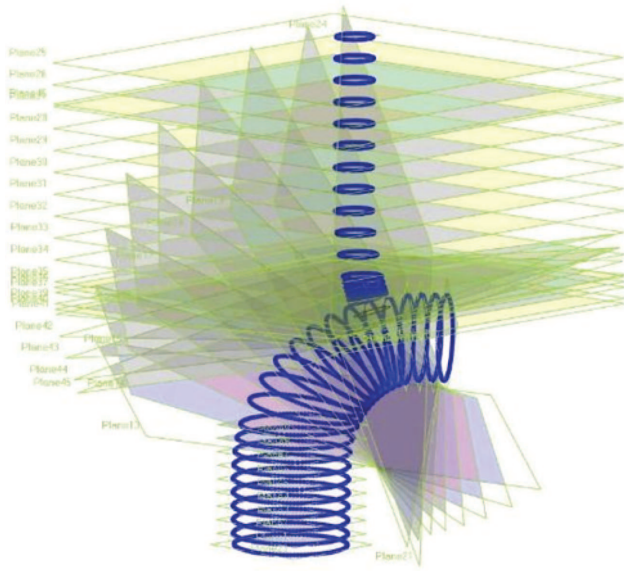


Figure 3: Planes and splines in Geometric Design X fitted to the scan data.

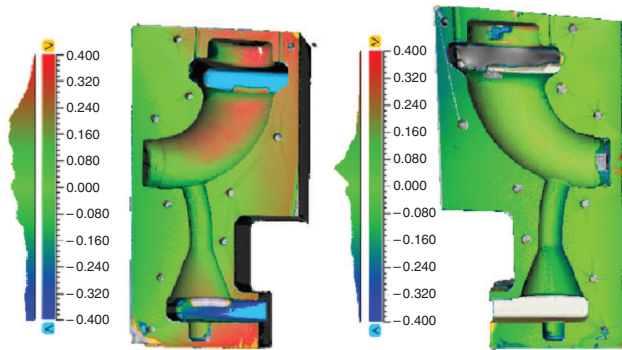


Figure 4: Difference between computational data and scan of the external mould in mm.

The internal mould was held in position by interference fits at each end of the internal mould (ascending aorta, brachiocephalic artery and peak of aortic arch). The internal mould was flexible enabling placement in the correct position relative to the external mould. Cyanoacrylate adhesive was used to fix the position of the internal mould. Figure 5 shows how the scanned model with the external mould compares to the manufactured parts.

2.4 Producing the phantom

The process described in Geoghegan et al. [10] was used to mitigate the incidence of bubble formation in the phantom. Dow Corning Sylgard 184 silicone was injected into

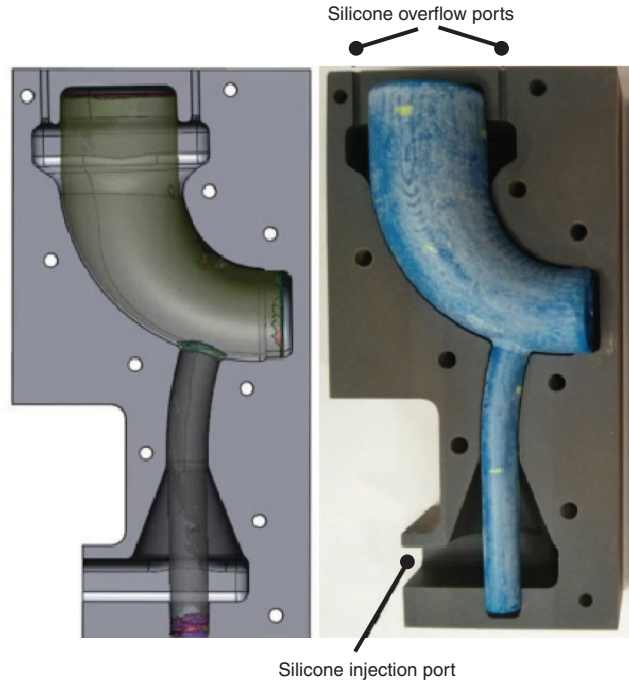


Figure 5: Internal mould in external mould in Geomagic Design X (left) and printed/machined model (right).

the lower port of the mould until it flowed out of the overflow ports indicating full investment of the mould. After 48 h of curing at room temperature (22°C), the external mould was removed. To vacate the internal mould, the phantom and internal mould was submerged in acetone for 48 h.

After PIV experimentation, the mould was dissected and the wall thickness of the mould was measured at 80 points on the aortic arch and 56 points on the brachiocephalic arch. Measurements were made using digital callipers. The smallest wall thickness was effectively zero. This occurred in the brachiocephalic artery (Figure 6). This rendered this part of the phantom useless for experimentation. The greatest wall thickness was 1.47 mm. This was 0.48 mm greater than the desired 0.99 mm in the aortic arch. The median wall thickness of the aortic arch walls was 1.01 mm, the minimum was 0.70 mm and the quartiles were 0.89 mm and 1.20 mm, respectively. The median wall thickness of the brachiocephalic artery was 0.58 mm (IQR 0.22 mm to 0.74 mm). This outcome implies that the internal mould was not centred properly during the pouring process.

The phantom refractive index matched the working fluid in Figure 7, which should effectively render the phantom invisible in the images [12]. The appearance of the phantom indicates that the surface finish on the phantom was not particularly smooth. Tactile inspection of

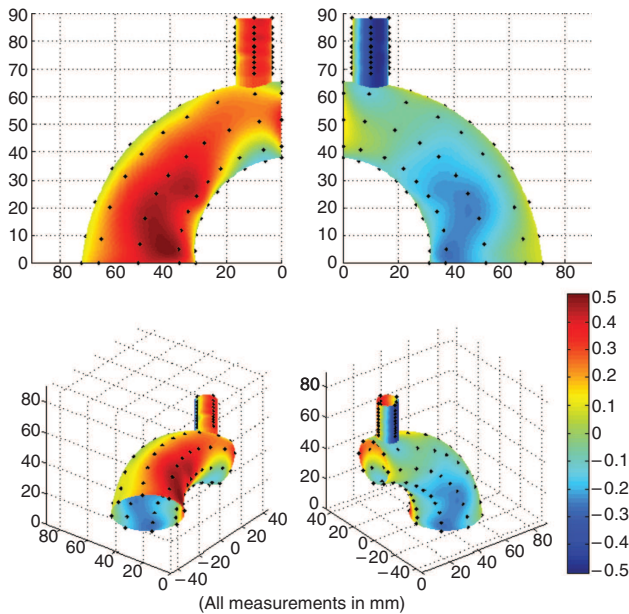


Figure 6: Deviation of the silicone mould from the desired wall thickness as measured at the black points.

the phantom indicated that the internal surface of the phantom was smooth, but the outer surface was rough.

The working fluid velocity field in the radial plane of the aortic arch was calculated using methods defined by Raffel et al. [13]. Figure 8 shows that at the lower edge the velocity is normal to the phantom. However, some vectors confound expected behaviour. In particular, it could be reasonably expected that the flow would be parallel to the phantom walls. It is expected that the surface roughness confounded the laser light plant and yielded erratic velocity fields that had insufficient fidelity to enable clinical research.

3 Conclusion

While additive manufacturing and 3D scanning technologies have been widespread for some time now, this research is the first of its kind to combine these technologies with traditional subtractive manufacturing and casting for the production of a biological phantom. In particular, this study describes a process for building thin walled, compliant silicone phantoms that contain complex shapes. Phantoms of this nature are critical to research wherein accurate representations of pulsatile flow fields are necessary, such as cardiac or pulmonary flow.

However, the lack of consistent wall-thicknesses in the phantom described and the surface roughness, the PIV imaging was not successful in terms of yielding usable

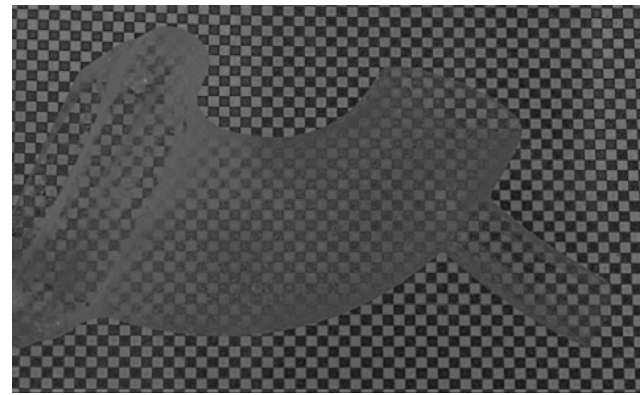


Figure 7: Refractive index matching phantom in the working fluid.

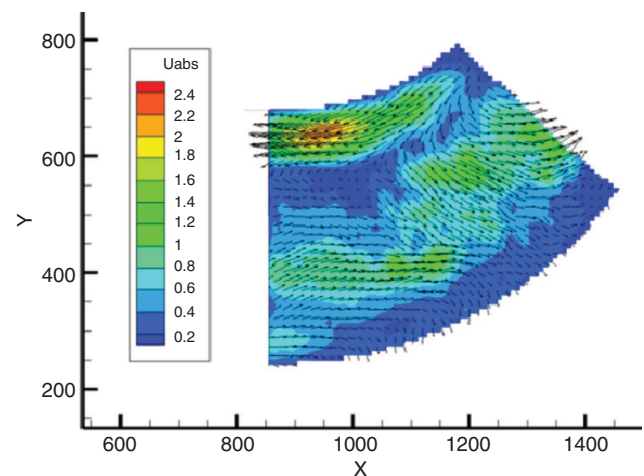


Figure 8: Velocity field in the aortic arch phantom.

data. However, the problems that we encountered should form important considerations for the academic community involved in experimental flow-imaging community.

Author's Statement

Research funding: The author state no funding involved. **Conflict of interest:** Authors state no conflict of interest. **Material and Methods:** Informed consent: Informed consent is not applicable. **Ethical approval:** The conducted research is not related to either human or animal use.

References

- [1] World Health Organisation. Cardiovascular Diseases (CVDs), Fact Sheet No. 317. World Health Organisation; 2015.
- [2] World Health Organisation. Cardiovascular Disease. Updated March 2013.
- [3] A.c. 2008, Australian and New Zealand Intensive Care Society (ANZICS) Centre for Outcome and Resource Evaluation (CORE),

- Annual Report. Australian and New Zealand Intensive Care Society (ANZICS) Centre for Outcome and Resource Evaluation (CORE). 2008.
- [4] A.c. 2010, Australian and New Zealand Intensive Care Society (ANZICS) Centre for Outcome and Resource Evaluation (CORE), 2010 Annual Report. Australian and New Zealand Intensive Care Society (ANZICS) Centre for Outcome and Resource Evaluation (CORE). 2010.
- [5] Sznajder M, Aegerter P, Launois R, Merliere Y, Guidet B, CubRea. A cost-effectiveness analysis of stays in intensive care units. *Intensive Care Med.* 2001;27:146–53.
- [6] Graf J, Muhlhoff C, Doig G, Reinartz S, Bode K, Dujardin R, et al. Health care costs, long-term survival, and quality of life following intensive care unit admission after cardiac arrest. *Critical Care.* 2008;12:R92.
- [7] Vincent J-L. [Fluid management: the pharmacoeconomic dimension.](#) *Critical Care* 2000;4:S33–5.
- [8] Caballero AD, Laín S. A review on computational fluid dynamics modelling in human thoracic aorta. *Cardiovascular Engineering and Technology.* 2013;4:103–30.
- [9] Biglino G, Verschueren P, Zegels R, Taylor AM, Schievano S. Rapid prototyping compliant arterial phantoms for in-vitro studies and device testing. *J Cardiovasc Magn Reson.* 2013;15:1–7.
- [10] Geoghegan P, Buchmann N, Spence C, Moore S, Jermy M. [Fabrication of rigid and flexible refractive-index-matched flow phantoms for flow visualisation and optical flow measurements.](#) *Exp Fluids.* 2012;52:1331–47.
- [11] Geoghegan P, Buchmann N, Soria J, Jermy M. [Time-resolved PIV measurements of the flow field in a stenosed, compliant arterial model.](#) *Exp Fluids.* 2013;54:1–19.
- [12] Huetter L, Geoghegan PH, Docherty PD, Lazarjan MS, Clucas D, Jermy MC. Application of a meta-analysis of aortic geometry to the generation of a compliant phantom for use in particle image velocimetry experimentation In: 9th IFAC Symposium on Biological and Medical Systems. Schauer T, editor. Berlin, Germany; 2015.
- [13] Raffel M, Willert C, Wereley S, Kompenhans J. Particle image velocimetry: a practical guide second edition. Berlin and New York; Springer; 2007.